

See discussions, stats, and author profiles for this publication at: <https://www.researchgate.net/publication/255963970>

# Kinetically Controlled Lithium-Staging in Delithiated LiFePO<sub>4</sub> Driven by the Fe Center Mediated Interlayer Li-Li Interactions

ARTICLE in CHEMISTRY OF MATERIALS · DECEMBER 2012

Impact Factor: 8.35 · DOI: 10.1021/cm3028324

---

CITATIONS

9

READS

45

## 5 AUTHORS, INCLUDING:



Xia Lu

McGill University

23 PUBLICATIONS 876 CITATIONS

[SEE PROFILE](#)



Ruijuan Xiao

Chinese Academy of Sciences

42 PUBLICATIONS 548 CITATIONS

[SEE PROFILE](#)



Hong Li

Chinese Academy of Sciences

274 PUBLICATIONS 10,298 CITATIONS

[SEE PROFILE](#)



Xuejie Huang

Chinese Academy of Sciences

192 PUBLICATIONS 6,147 CITATIONS

[SEE PROFILE](#)

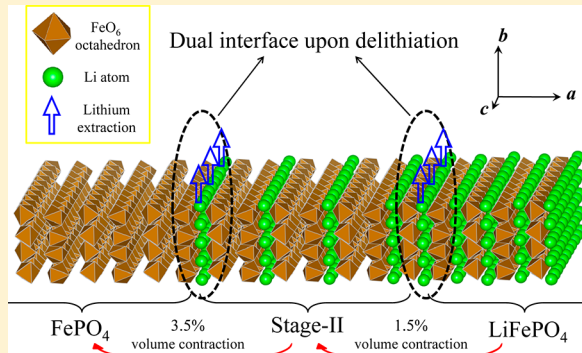
# Kinetically Controlled Lithium-Staging in Delithiated LiFePO<sub>4</sub> Driven by the Fe Center Mediated Interlayer Li–Li Interactions

Yang Sun, Xia Lu, Ruijuan Xiao, Hong Li, and Xuejie Huang\*

Beijing National Laboratory for Condensed Matter Physics, Institute of Physics, Chinese Academy of Sciences, Beijing 100190, China

**ABSTRACT:** Employing density functional theory (DFT) calculations, we demonstrate that the stage-II configuration in delithiated LiFePO<sub>4</sub> is a thermodynamically metastable but kinetically controlled state, distinct from the thermodynamically favorable stages in graphite intercalation compounds (GICs). Based on the computational results, we propose a dual-interface model to describe the delithiation mechanism of LiFePO<sub>4</sub> upon charging. Accordingly, the experimentally observed LiFePO<sub>4</sub>/stage-II/FePO<sub>4</sub> three-phase coexistence could be successfully reproduced. Formation of lithium-staging configuration is mainly attributed to the Fe center mediated interlayer Li–Li interactions, which is an essential indirect electrostatic force. The indirect interaction originates from the localized nature of Fe 3d electrons, for which the effective oxidation state of Fe redox is determined by the Li ion arrangement and, in turn, has an impact on the behavior of Li ion diffusion. Besides a better understanding of the microscopic lithium diffusion mechanism in LiFePO<sub>4</sub>, our results also shed light on the interactions between electron and ion and further emphasize the importance of studying the Li diffusion kinetics at phase boundary in phase separation materials.

**KEYWORDS:** olivine LiFePO<sub>4</sub>, lithium staging, lithium ion diffusion kinetics, density functional theory calculations, Li ion batteries



## INTRODUCTION

Being a commercialized cathode material of Li ion batteries for electric vehicles,<sup>1,2</sup> olivine-structured LiFePO<sub>4</sub> has undergone intensive research since the pioneering work by Padhi et al.<sup>3</sup> It is reported that LiFePO<sub>4</sub> exhibits a two-phase separation reaction,<sup>3,4</sup> displaying a voltage plateau at 3.45 V vs Li<sup>+</sup>/Li with theoretical specific capacity of 170 mAh/g. During charging, Li<sup>+</sup> ions are extracted from LiFePO<sub>4</sub> cathode to the anode (e.g., graphite) across the ionic conducting but electronic insulating electrolyte (normally consisting of Li salts dissolved in organic solvents), with the compensating electrons traversing an external electronic circuit and vice versa upon discharging. The major limitation of the LiFePO<sub>4</sub> cathode material lies in its low intrinsic electronic and ionic conductivities. However, there, drawbacks have been improved much from both experimental and theoretical aspects. On the one hand, surface modifications, particularly by the carbon coating techniques, have been successfully used to overcome the insulating nature of LiFePO<sub>4</sub> by constructing an effective conduction network for the electron transfer.<sup>5–7</sup> On the other hand, considerable efforts have been devoted to understanding the mechanism of Li transport in order to further enhance the rate capability of LiFePO<sub>4</sub>.

One-dimensional lithium diffusion along the (010) direction of LiFePO<sub>4</sub> was first predicted by first-principles calculations<sup>8–10</sup> and later confirmed by neutron diffraction experiment.<sup>11</sup> As the LiFePO<sub>4</sub> electrode shows a typical two-phase reaction, the distribution of the two phases, LiFePO<sub>4</sub> and

FePO<sub>4</sub>, upon charging/discharging is a focus of research. Various models, including the core–shell model,<sup>3</sup> the mosaic model,<sup>4,12</sup> the shrinking core model,<sup>13</sup> and the domino-cascade model<sup>14</sup> were proposed to describe the phase evolution of a single LiFePO<sub>4</sub> particle during the electrochemical delithiation process. Regardless of different nucleation sites, it is generally accepted that, in charging processes, Li ions are extracted along [010] direction accompanied by the LiFePO<sub>4</sub>/FePO<sub>4</sub> phase boundary moving along the *a*-axis.<sup>14–16</sup> However, detailed Li ion diffusion on the two-phase interface region has not been clarified sufficiently. Besides, this is of crucial importance in improving the electrochemical properties of LiFePO<sub>4</sub> electrode.

Previously, the Li diffusion mechanism in LiFePO<sub>4</sub> was commonly illustrated by the Li-rich and the Li-poor phases at room temperature<sup>17–19</sup> and/or the Li<sub>x</sub>FePO<sub>4</sub> ( $0 < x < 1$ ) solid solution at high temperature (or in nanosizing particle).<sup>20–22</sup> However, recent discovery indicates a more subtle atomic structure (i.e. lithium-staging phenomenon),<sup>23</sup> which is beyond the conventional two-phase wisdom. That is difficult to understand in theory, as two-phase separation was calculated to be the energetically favorable configuration at room temperature.<sup>24</sup> Assuming a single-phase LiFePO<sub>4</sub> transformation path, Malik et al. obtained the staging-like configuration through Monte Carlo simulations,<sup>25</sup> while the underlying

Received: September 3, 2012

Revised: November 19, 2012

Published: November 20, 2012

mechanism was not rationalized. More recently, a LiFePO<sub>4</sub>/lithium-staging/FePO<sub>4</sub> three-phase boundary was observed in a partially chemically delithiated LiFePO<sub>4</sub> sample.<sup>26</sup> These results are in contradiction with the classical continuum model with diffuse interface<sup>13,27–31</sup> and thereby further challenge the current understanding on the formation and migration of phase boundary in LiFePO<sub>4</sub>. Our new contribution aims to reveal the origin of this lithium-staging phenomenon and to further explore possible atomic structure on the LiFePO<sub>4</sub>/FePO<sub>4</sub> boundary by first-principles calculation based on density functional theory (DFT).

## METHOD

Spin-polarized calculations were performed using the Vienna ab initio simulation package (VASP)<sup>32,33</sup> within the projector augmented-wave approach.<sup>34</sup> Generalized gradient approximation (GGA) in the parametrization of Perdew, Burke, and Ernzerhof (PBE)<sup>35</sup> pseudopotential was used to describe the exchange–correlation potential and a Hubbard-type correction U was taken into account due to the strongly correlated nature of the Fe 3d electrons.<sup>36,37</sup> This GGA+U method has already been validated by satisfactorily reproducing many properties of LiFePO<sub>4</sub>.<sup>24,38–43</sup> According to a previous work, the effective U value was set to 4.3 eV.<sup>38</sup> A kinetic energy cutoff of 520 eV was used in all calculations. Geometry optimizations were performed by using a conjugate gradient minimization until all the forces acting on ions were less than 0.01 eV/Å per atom. K-point mesh with a spacing of ca. 0.03 Å<sup>-1</sup> was adopted. Although the ground state of LiFePO<sub>4</sub> is antiferromagnetic, herein we adopt the ferromagnetic spin configuration to simplify the problem in all calculations as the spin sequence has negligible impact on the activation barriers.<sup>8</sup>

Minimum energy pathways and saddle points of Li<sup>+</sup> migration or small polaron hopping were calculated with the climbing-image nudged elastic band (CINEB) method.<sup>44</sup> This approach duplicates a series of images (seven images in our calculations) between the starting point and the end point of diffusing ion to simulate the intermediate states, with the positions of the starting point and the end point fixed. For the polaron hopping process, we adopt the same method described in ref 45, wherein the polaron hopping is described by a transfer of lattice distortion. A 3a × 2b × 2c (S.G. *Pnma*) supercell containing 48 formula units is used to minimize the interactions between periodic images. For the large supercell adopted in CINEB calculations, only the  $\Gamma$  point is adopted for k-point sampling to reduce the computational cost. The convergence check indicates that a denser k-mesh does not affect our conclusion qualitatively.

Even though it has been shown that solid solution regions exist nearby the end-members of Li<sub>x</sub>FePO<sub>4</sub>, we adopted idealized models consisting of fully delithiated and lithiated phases, viz. LiFePO<sub>4</sub> and FePO<sub>4</sub>. In the calculations, the sites on which the excess electron/hole is localized are sensitive to the starting configurations, leading to multiple local energy minima for a given supercell. Nonetheless, the charge localization could be controlled by adjusting the initial ionic position, and accordingly, we try various configurations of the electrons localized on the Fe centers to obtain the lowest energy state.

## RESULTS

**Thermodynamic Calculations.** Originally, the staging phenomenon is used to describe the periodical arrangements of the intercalant (Li, K, HNO<sub>3</sub>, AsF<sub>5</sub>, etc.) in GICs.<sup>46–48</sup> Here, for LiFePO<sub>4</sub>, if neglecting the connective PO<sub>4</sub> tetrahedra, its structure can also be regarded to be a layered structure perpendicular to the *a*-axis with the alternating Fe–O and Li–O slabs. Using the same staging definition as in GICs, a fully lithiated iron phosphate (LiFePO<sub>4</sub>) corresponds to the stage-I configuration, as schematically illustrated in Figure 1. For the

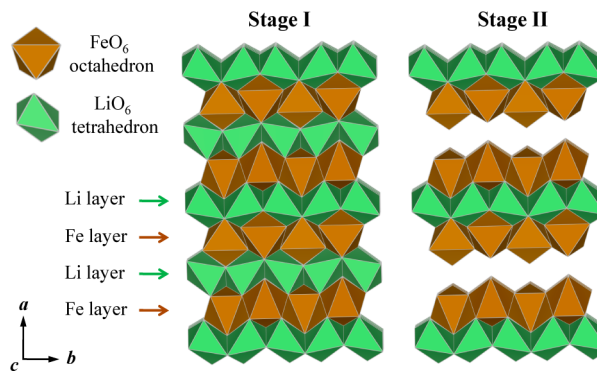


**Figure 1.** Schematic representation of the stage-I (LiFePO<sub>4</sub>) and stage-II (Li<sub>0.5</sub>FePO<sub>4</sub>) configurations, where only FeO<sub>6</sub> octahedra (brown) and LiO<sub>6</sub> tetrahedra (green) are demonstrated for a convenient visualization.

half-delithiated LiFePO<sub>4</sub> (nominal Li<sub>0.5</sub>FePO<sub>4</sub>), the aberration-corrected spherical scanning transmission electron microscopy (STEM) images showed that the contrast of Li columns vanished at every other layer,<sup>23</sup> indicating a stage-II configuration. To check the thermodynamic stability of this configuration, we calculated the formation energies of Li<sub>0.5</sub>FePO<sub>4</sub> with the conventional two-phase-coexisting model and stage-II model, respectively. The results in Figure 2 indicate that the formation energy of the two-phase-coexisting model increases with decreasing supercell size. Nevertheless, even for the smallest supercell 2a with the largest interface energy, the formation energy of the two-phase-coexisting model is lower than that of the stage-II model. That is, the stage-II configuration is always energetically unstable against two-phase separation, regardless of the size of the simulated supercell. Thermodynamically, a stoichiometric Li<sub>0.5</sub>FePO<sub>4</sub> particle tends to adopt a two-phase-coexisting structure rather than the stage-II structure. Therefore, experimental observation of the stage-II structure in half-delithiated Li<sub>0.5</sub>FePO<sub>4</sub> sample implies that the kinetic transformation path should deviate from the equilibrium phase diagram, in which no other ordered phase beyond LiFePO<sub>4</sub> and FePO<sub>4</sub> is expected. Accordingly, the kinetics related to the Li extraction process should be investigated.

**Kinetic Calculations.** Before the kinetic calculations, we first consider the case of creating one lithium vacancy (V<sub>Li</sub><sup>/</sup> in Kröger–Vink notation). Owing to the strongly correlated 3d orbitals, Fe ions undergo an oxidation from Fe<sup>2+</sup> to Fe<sup>3+</sup>,<sup>38</sup> and thereby, removal of one Li atom is equivalent to creating a V<sub>Li</sub><sup>/</sup> and a localized hole (h<sup>•</sup>) on Fe redox center simultaneously. This would induce lattice distortion around the trivalent Fe center forming a small polaron, which can be deemed as a quasi-particle.<sup>24</sup> The Li diffusion in Li<sub>x</sub>FePO<sub>4</sub> is a combination of the Li<sup>+</sup> migration and the small polaron hopping, which has

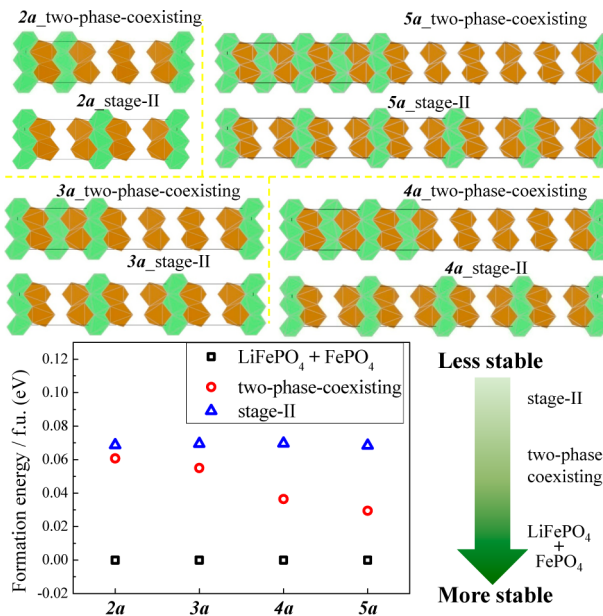


**Figure 2.** Calculated formation energy (versus isolated  $\text{LiFePO}_4$  and  $\text{FePO}_4$  two phases) of  $\text{Li}_{0.5}\text{FePO}_4$  with the conventional two-phase-coexisting model and stage-II model. The formation energy is defined as  $E'(\text{Li}_{0.5}\text{FePO}_4) = E(\text{Li}_{0.5}\text{FePO}_4) - 1/2[E(\text{LiFePO}_4) + E(\text{FePO}_4)]$ , wherein  $E(\text{Li}_{0.5}\text{FePO}_4)$ ,  $E(\text{LiFePO}_4)$ , and  $E(\text{FePO}_4)$  represent the supercell energies of  $\text{Li}_{0.5}\text{FePO}_4$ ,  $\text{LiFePO}_4$ , and  $\text{FePO}_4$ , respectively. As shown in the upper panel, we use the simulated supercell of different sizes as follows: extending  $\text{LiFePO}_4$  unitcell along the  $a$ -axis direction by  $X$  times is labeled as  $Xa$ . All supercells are depicted along  $c$  projection, and the color scheme is consistent with Figure 1.

been demonstrated both in theory and experiment.<sup>20,45,49</sup> Therefore, it was divided into several elementary steps in the following calculations. That is, during the  $\text{Li}^+$  migration process, the  $\text{Fe}^{3+}$  polaron keeps its position unchanged, and vice versa.<sup>50</sup> In particular, for a given  $\text{Li}/\text{V}_{\text{Li}}$  arrangement, there are multiple configurations as the  $h^\bullet$  may localize on different Fe centers, while the ground-state corresponds to the configuration that the  $h^\bullet$  is adjacent to the  $\text{V}_{\text{Li}}^\circ$ , viz. the adjacent  $\text{Fe}^{2+}$  in  $\text{LiFePO}_4$  are oxidized to  $\text{Fe}^{3+}$  upon Li extraction. Within the perfect  $\text{LiFePO}_4$ , one Li ion has two nearest neighboring Fe centers, which are crystallographically equivalent. Consequently, once a Li ion is removed, the electron will be compensated by one of the two adjacent Fe centers, each with 50% probability.

The Li diffusion kinetics in  $\text{LiFePO}_4$  bulk could be assessed by removing one Li atom from a perfect  $\text{LiFePO}_4$  supercell and then calculating the energy barriers of above-mentioned elementary steps, that is, the  $\text{Li}^+$  migration step and the small polaron hopping step. Here, the energy barrier refers to the difference in energy between the saddle point along the hopping pathway and the initial minimum. As shown in Figure 3b, Li sites and Fe centers are denoted by  $\text{Ln}$  and  $\text{Fn}$  ( $n = 1, 2, 3$ ), respectively. The  $\text{LnFn}$  complex represents the configuration that a  $\text{V}_{\text{Li}}^\circ$  resides in  $\text{Ln}$  site and the  $h^\bullet$  is localized at  $\text{Fn}$  center. Two  $\text{Li}^+$  migration steps ( $\text{L1F1} \rightarrow \text{L2F1}$ ,  $\text{L2F2} \rightarrow \text{L3F2}$ ) and two polaron hopping steps ( $\text{L2F1} \rightarrow \text{L2F2}$ ,  $\text{L3F2} \rightarrow \text{L3F3}$ ) constitute a complete Li diffusion process  $\text{L1F1} \rightarrow \text{L2F1} \rightarrow \text{L2F2} \rightarrow \text{L3F2} \rightarrow \text{L3F3}$ . Actually,  $\text{L1F1} \rightarrow \text{L2F1} \rightarrow \text{L2F2}$  is a repetitive unit that could be used to describe the whole Li diffusion process; here, we show two units for the convenience of comparing with subsequent calculations. It can be seen that, at each stable configuration (i.e.  $\text{L1F1}$ ,  $\text{L2F1}$ ,

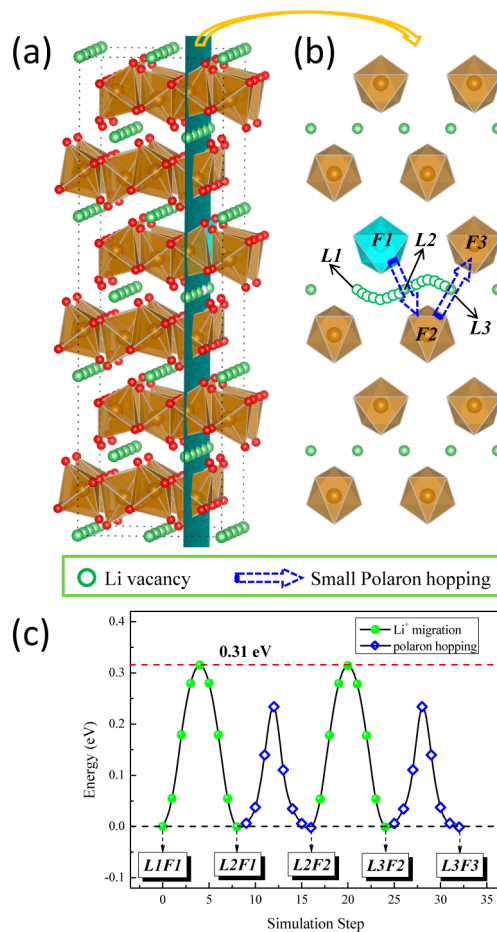


**Figure 3.** Lithium diffusion process in the  $\text{LiFePO}_4$  bulk. (a) The  $\text{LiFePO}_4$  supercell used in our calculation. Only  $\text{FeO}_6$  octahedra and Li atoms are plotted, with brown surfaces and green balls, respectively. Oxidized  $\text{FeO}_6$  octahedra are light blue. (b) A (001) slice cut from part a, where the  $\text{Li}^+$  migration and small polaron hopping process are represented by green circles and dashed blue arrows, respectively. (c) Calculated energy barriers with respect to the simulation steps shown in part b.

$\text{L2F2}$ ,  $\text{L3F2}$ , and  $\text{L3F3}$ ), the corresponding total energies are degenerated to the same level. That is easy to understand, as the supercell is highly symmetric and hence all of these configurations have equivalent crystallographic coordinates, resulting in the identical supercell energy. Energy barriers of  $\text{Li}^+$  migration and small polaron hopping are calculated to be 0.31 and 0.23 eV, respectively, in line with the previous reported values.<sup>8,45,51</sup> Accordingly, the activation energy associated with the overall Li diffusion process is ca. 0.31 eV along [010] direction in  $\text{LiFePO}_4$  lattice (Figure 3c). Under the assumption that the Li ion moves to its nearest-neighbor vacancy site along the 1D Li channel, the diffusion coefficient can be estimated based on the following equation:<sup>8</sup>

$$D = a^2 v \exp(-E_{\text{act}}/k_{\text{B}}T)$$

where  $a$  is the hopping length, which is ca. 3 Å in this case;  $v$  is the attempt frequency and a typical value of  $10^{12}$  Hz is used here;  $k_{\text{B}}$  is the Boltzmann constant;  $T$  is the temperature (300 K at room temperature);  $E_{\text{act}}$  is the diffusion barrier, which could be predicted by first-principles calculation, as shown above. Consequently, the diffusion coefficient is calculated to be ca.  $5.5 \times 10^{-9} \text{ cm}^2/\text{s}$ .

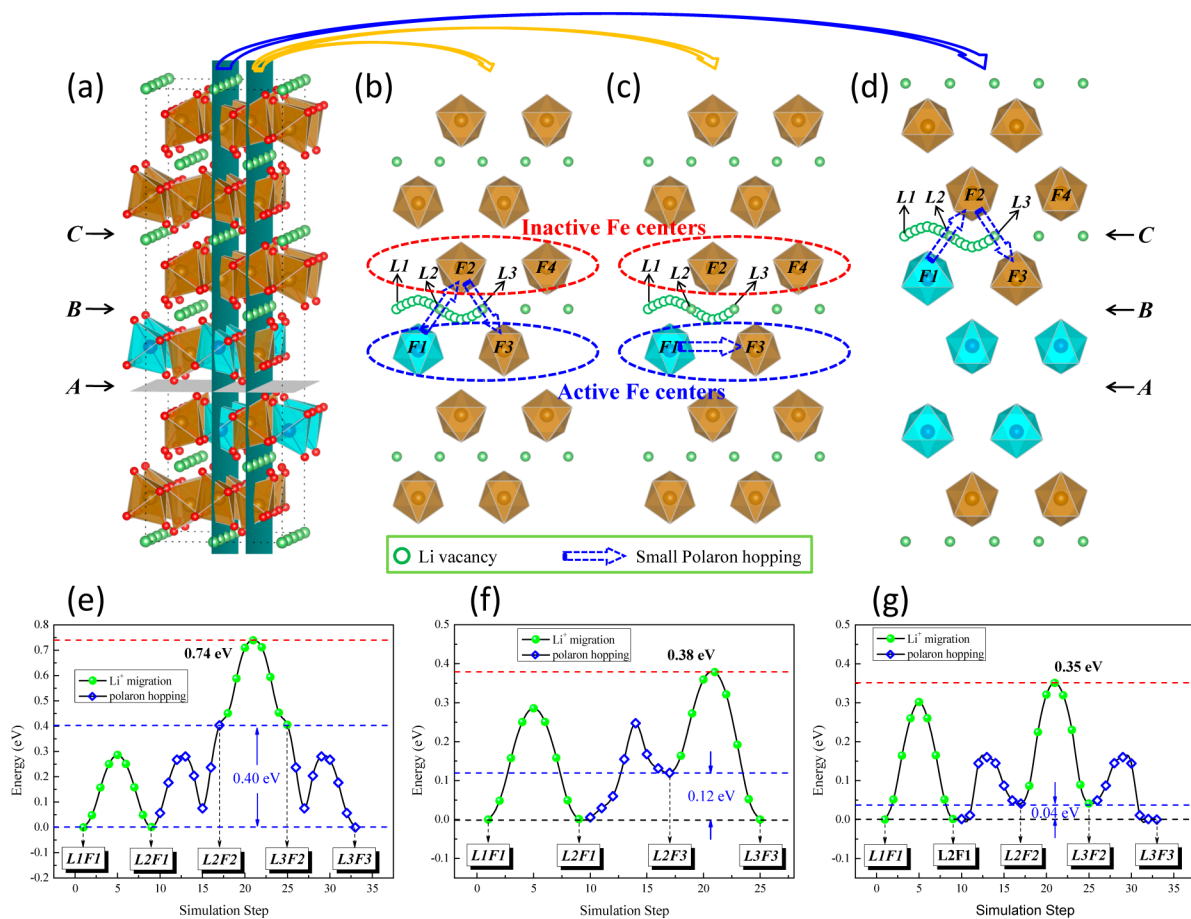


**Figure 4.** Lithium diffusion process after one Li layer (l-A) is emptied. The color scheme is consistent with Figure 2. (a) Adopted LiFePO<sub>4</sub> supercell, with l-A emptied. (b–d) The (001) slices cut from part a. (e–g) Calculated energy barriers with respect to the simulation steps as shown in parts b–d.

Then, we consider the Li diffusion kinetics after one Li layer (labeled as l-A) is removed. As shown in Figure 4a, the ground-state is achieved when all Fe ions nearest to Li vacancies are oxidized to Fe<sup>3+</sup>. Adopting the same steps as used in the bulk case (Figure 4b), a significantly higher energy barrier of 0.74 eV is obtained (Figure 4e). This corresponds to a diffusion coefficient of  $3.3 \times 10^{-16}$  cm<sup>2</sup>/s, which is 7 orders of magnitude lower than the bulk value, implying that this Li diffusion is nearly impossible. Such a large energy barrier is mainly contributed by the polaron hopping step from L2F1 to L2F2, as there is a large energy difference between the L2F1 pair and the L2F2 pair. That is due to the fact that the two previously equivalent Fe centers, F1 and F2 in Figure 3b, experience different chemical environments after the presence of one Li vacancy layer (l-A). If a V<sub>Li</sub><sup>+</sup> is created at L2 site in the Li l-B layer in Figure 4b, the resulting h<sup>•</sup> prefers to be localized on F1 (L2F1) other than F2 (L2F2) by an energy advantage of ca. 0.40 eV (the cause of this energy difference will be analyzed in detail below). As a result, the h<sup>•</sup> is much more likely to localize on Fe centers adjacent to Li l-A layer (F1, F3, ...), the number of which accounts for half of all Fe centers, making these Fe centers active as Fe<sup>2+</sup>/Fe<sup>3+</sup> redox (marked by blue dotted circle in Figure 4b, c), while the other half of the Fe centers (F2, F4, ...), away from Li l-A layer, remains inactive during the Li diffusion process (marked by red dotted circle in Figure 4b, c). Naturally, we may construct another possible path (i.e. L1F1 → L2F1 → L2F3 → L3F3 (Figure 4c)) by utilizing the active Fe

centers. This diffusion path results in an energy barrier of 0.38 eV (Figure 4f), slightly higher than the bulk value (corresponding to a diffusion coefficient of  $3.7 \times 10^{-10}$  cm<sup>2</sup>/s) and hence seems to be a feasible solution for Li diffusion in Li l-B layer. However, it should be noted that, in this path, the L2F3 pair represents the configuration that the Fe<sup>3+</sup> polaron (F3) is second nearest to the V<sub>Li</sub><sup>+</sup> (L2), contrary to the bulk case wherein the h<sup>•</sup> localizes on the Fe center nearest to the corresponding V<sub>Li</sub><sup>+</sup> after each hopping step. More importantly, the L2F1 → L2F3 hopping in Figure 4c requires the occupation of Li ion at the L3 site as a prerequisite; otherwise, a V<sub>Li</sub><sup>+</sup> at L3 site will lead to a h<sup>•</sup> localized on the F3 center, which blocks the hopping and thus invalidates this diffusion path. Consequently, a slow Li diffusion kinetics could be expected given the existence of a certain number of V<sub>Li</sub><sup>+</sup>s, for lacking available redox centers. This constraint is nonexistent in the Figure 3b, where the one-to-one relationship between the Li ion and Fe redox center ensures a sufficient number of polarons, which is necessary for a facile Li diffusion process. Considering that only half of the Fe centers are active, at most half of the Li atoms in Li l-B layer might be extracted; nevertheless, this is unrealistic, as then an uniform Li/V<sub>Li</sub><sup>+</sup> distribution along the b direction is needed to reach the minimum energy state, which could be hardly to achieve owing to the one-dimensional nature of the Li channel. For these reasons, the Li diffusion is not likely to follow the migration path in Figure 4c, even though the related activation energy is not very high. As remarked above, the

kinetics of Li diffusion in the Li l-B layer becomes slow once the Li ions in l-A layer have been removed.

We further investigate the diffusion kinetics of Li ion in the second adjacent Li layer (l-C). Following the migration path L1F1 → L2F1 → L2F2 → L3F2 → L3F3, as shown in Figure 4d, the overall energy barrier of is calculated to be 0.35 eV (Figure 4g). Here, the polaron hopping step from L2F1 to L2F2, which greatly increased the overall Li diffusion energy barrier in Figure 4e, only raises the activation energy by 0.04 eV. Thus, the calculated diffusion coefficient is  $1.2 \times 10^{-9} \text{ cm}^2/\text{s}$ , which is the same level as the bulk value. This indicates that the Li vacancy layer has little effect on the Li diffusion in its second nearest Li layer, and as a result, a comparably facile lithium extraction is expected. Therefore, after the Li ions in l-A layer have been extracted, the subsequent delithiation process will preferentially proceed in l-C rather than l-B layer.

Supposing that the Li ions in both l-A and l-C layers are removed (Figure 5a), we reevaluate the Li diffusion kinetics in the Li l-B layer. As can be seen in Figure 5b, the two Fe centers nearest to L2 (i.e. F1 and F2), the equity of which was broken by the appearance of one Li vacancy layer in Figure 4b, become equivalent again. Consequently, the energy gap between the L2F1 pair and the L2F2 pair returns to zero. Following the

same trajectory adopted in Figure 4b, the activation energy of the whole Li diffusion process is calculated to be 0.32 eV (Figure 5b, c), leading to a diffusion coefficient of  $3.7 \times 10^{-9} \text{ cm}^2/\text{s}$ . This suggests that the Li diffusion in l-B layer is reactivated after the two adjacent Li layers are both removed.

The computational results show that the activation energy of Li diffusion changes as a response to the occupancy of its adjacent Li layers (for l-B layer, the adjacent layers are l-A and l-C). After one and only one of its two adjacent Li layer is removed, the Li diffusion kinetics becomes slow; a facile Li diffusion process could be realized only when both adjacent layers are either occupied by Li ions or left unoccupied. As mentioned earlier, this relation lies primarily in the energy difference between the L2F1 pair and the L2F2 pair. In Figure 3, where both the Li l-A and l-C layers are occupied by Li ions, the energies of L2F1 and L2F2 are degenerated, and therefore, the polaron hopping from L2F1 to L2F2 is not an obstacle for the Li diffusion process. After the Li ions in l-A layer are removed in Figure 4, the L2F1 pair is more energetically favorable than the L2F2 pair by 0.40 eV, resulting in a high activation energy for the overall Li diffusion process. Here, the energy difference between L2F1 and L2F2 is caused by the coordination symmetry broken of two previously equivalent Fe centers. As schematically illustrated in Figure 6, the overall

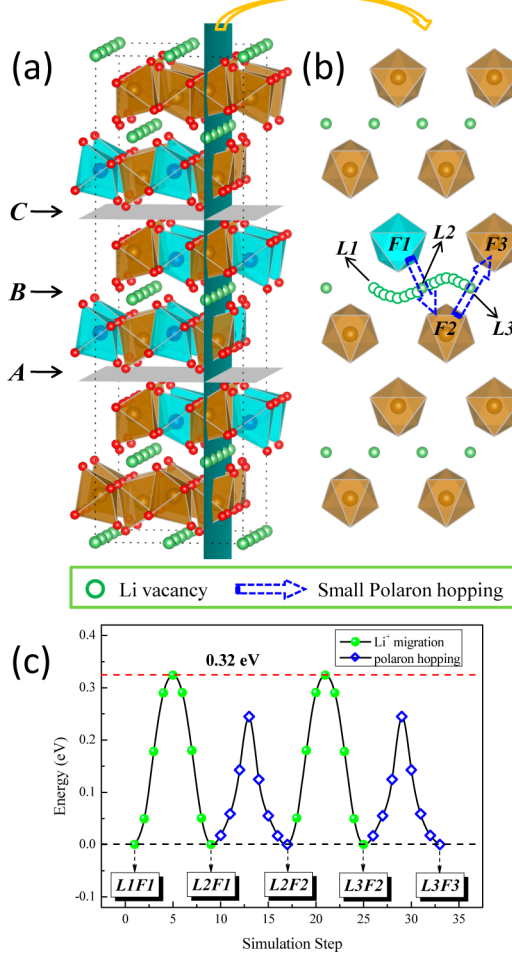


**Figure 5.** Li diffusion process after both l-A and l-C are emptied. The color scheme is consistent with Figure 2. (a) Adopted LiFePO<sub>4</sub> supercell, with l-A and l-C emptied. (b) A (001) slice cut from part a. (c) Calculated energy barriers with respect to the simulation steps as shown in part b.

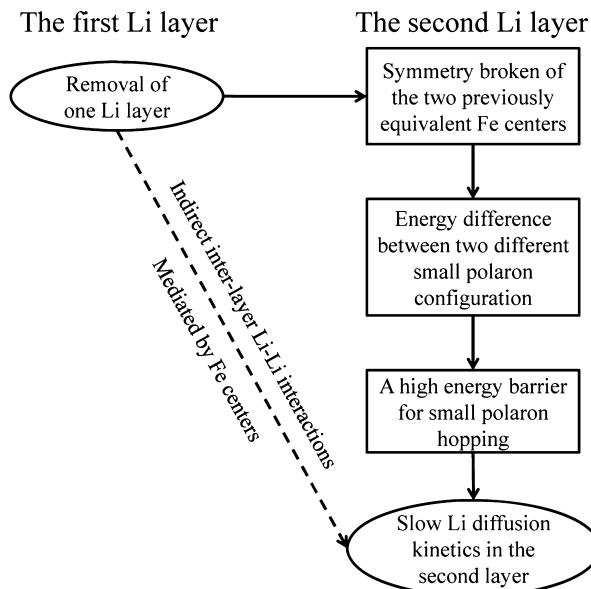


**Figure 6.** Schematic view of the indirect interlayer Li–Li interaction mediated by Fe centers.

effect is equivalent to an interlayer Li–Li interaction, which is essentially an indirect electrostatic force mediated by Fe centers. Given that the Li ions in both l-A and l-C layers are removed, the geometric symmetry resumes and the energy gap between L2F1 and L2F2 disappears; as a result, the facile Li diffusion in Li l-B layer is regained, as shown in Figure 5.

The energy difference between L2F1 and L2F2 in Figure 4b, caused by the broken symmetry of the two previously equivalent Fe centers, originates from the highly localized nature of Fe 3d electrons. As is well-known, LiFePO<sub>4</sub> is a strongly correlated system with highly localized Fe 3d electrons, and therefore, only by considering the localized nature of Fe 3d electrons can we reproduce the band gap,<sup>39</sup> insertion voltage,<sup>38</sup> and phase separation characteristic.<sup>52</sup> Localized Fe 3d electrons

lead to localized  $\text{Fe}^{2+}/\text{Fe}^{3+}$  redox center, the effective oxidation state of which is determined by the arrangement of  $\text{Li}^+/\text{V}_{\text{Li}}^+$  on its adjacent Li site. In ref 24, Zhou et al. have shown that phase separation in  $\text{Li}_x\text{FePO}_4$  is mainly driven by the  $\text{Li}^+-\text{Fe}^{2+}$  attraction. To confirm this relationship, we calculate the supercell energies as a function of the distance between the  $\text{Li}^+-\text{Fe}^{2+}$  ( $\text{V}_{\text{Li}}^+-\text{Fe}^{3+}$ ) pair in  $\text{LiFePO}_4$  ( $\text{FePO}_4$ ). Results in Figure 7 show that the formation energy increases with the pair

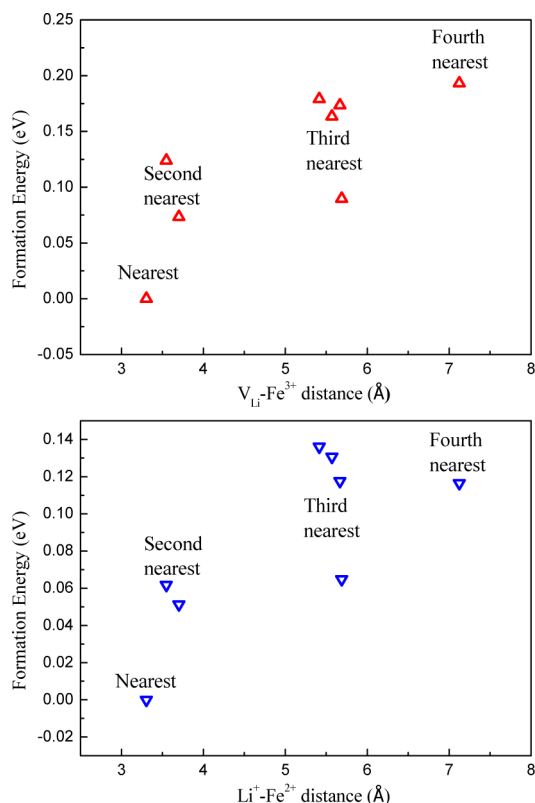


**Figure 7.** Formation energy of the  $\text{V}_{\text{Li}}^+/\text{Fe}^{3+}$  ( $\text{Li}^+/\text{Fe}^{2+}$ ) pair in  $\text{LiFePO}_4$  ( $\text{FePO}_4$ ) supercell, as a function of the pair distances.

distance, thus illustrating the strongly bounded  $\text{Li}^+/\text{Fe}^{2+}$  ( $\text{V}_{\text{Li}}^+/\text{Fe}^{3+}$ ) pair. That may explain the energy difference between L2F1 and L2F2 configurations: If the F1 center is oxidized to  $\text{Fe}^{3+}$ , as schematically illustrated in Figure 8a, then  $\text{Fe}^{2+}$  at the F2 center is encompassed with Li ions and  $\text{Fe}^{3+}$  at the F1 center is largely surrounded by  $\text{V}_{\text{Li}}^+$ , constituting the energetically favorable state; otherwise, assuming F2 center is oxidized to  $\text{Fe}^{3+}$  while F1 remains  $\text{Fe}^{2+}$  (Figure 8b), it shows that  $\text{Fe}^{2+}$  and  $\text{Fe}^{3+}$  are trapped by  $\text{V}_{\text{Li}}^+$  and Li ions, respectively, making this configuration energetically unfavorable.

For comparison, we also performed standard GGA calculations without U correction (not shown here). Pure GGA is insufficient to treat electron correlation, leading to delocalized 3d electrons. In the framework of standard GGA, the calculated activation energy of Li diffusion is nearly independent of the occupancy state of its adjacent Li layer, further proving that the indirect interlayer Li-Li interaction is closely related to the localized nature of Fe 3d electrons.

**Schematic Models for Delithiation.** Summarizing the above calculations and analysis, possible microscopic mechanisms can be inferred for the Li ion diffusion process upon charging. As a phase separation reaction, the delithiation process in  $\text{LiFePO}_4$  is accompanied by the movement of the

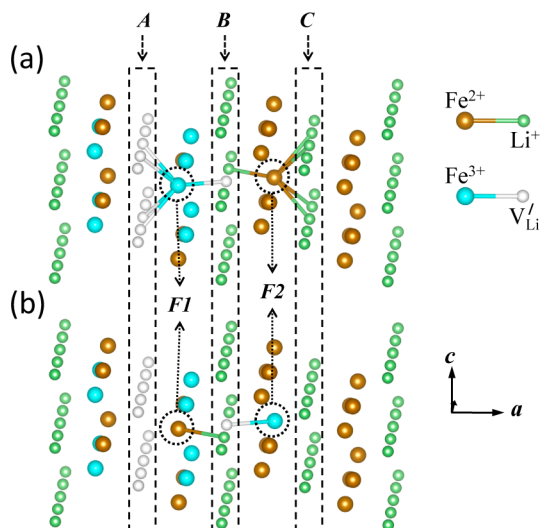


**Figure 8.** Schematic illustration of the L2F1 (a) and L2F2 (b) configurations, after a Li vacancy layer has been created.  $\text{Li}^+$ ,  $\text{V}_{\text{Li}}^+$ ,  $\text{Fe}^{2+}$ ,  $\text{Fe}^{3+}$  are represented by green, white, brown, light blue balls, respectively. The attractive  $\text{Li}^+-\text{Fe}^{2+}$  and  $\text{V}_{\text{Li}}^+-\text{Fe}^{3+}$  (only for Fe at the F1 and F2 centers) pairs less than 4.0 Å are plotted.

phase boundary along the  $a$ -axis, which could be described as a delithiation wave, and the driving force is related to the lattice mismatch between different phases.<sup>14</sup> Here, we assume that the delithiation wave could go through the whole  $\text{LiFePO}_4$  particle once it is formed. Surely this assumption does not apply to a large particle, which has more than one nucleation site (where the delithiation wave is initiated) upon charging. Nevertheless, a large particle could be considered to consist of many small grains, and their delithiation processes are nearly independent. To facilitate comprehension, the Li layers are labeled in alphabetical order in Figure 9a. Given that the delithiation process initially happens from the Li l-A layer, the following Li extraction in the l-B layer will be impeded due to a high small polaron hopping barrier. As a result, the subsequent Li extraction will possibly be started at the l-C layer. Then, the Li ions in both l-A and l-C layers are emptied, the next delithiation procedure may occur at one of the two Li layers (i.e. the l-B layer or the l-E layer). In the former case, the delithiation sequence of A-C-E-G-I is shown in Figure 9b and denoted as EX-I; in the latter case, the delithiation sequence of A-C-B-E-D is shown in Figure 9c and denoted as EX-II. Actually, EX-I and EX-II are two extreme cases, as each of them follows a single delithiation sequence. For the EX-I model, the delithiation wave propagates in a single direction. At the half-delithiated state, the delithiation wave has gone through the whole particle and result in  $\text{Li}_{0.5}\text{FePO}_4$  with the stage-II configuration. Further charging will initiate another delithiation wave of B-D-F-H-J, which ultimately converts the stage-II into  $\text{FePO}_4$ . The EX-II model depicts a scenario of the delithiation wave moves back-and-forth upon charging, leading to a two-phase coexisting configuration with a sharp  $\text{LiFePO}_4/\text{FePO}_4$  boundary. The sharp two-phase boundary could also result from another extreme delithiation scheme of EX-III (Figure 9d), which gives a picture of two delithiation waves (A-C-E-G-I and B-D-F-H-J) moving forward synchronously.

By combining the above-mentioned extreme cases, we could also construct the delithiation models illustrated in Figure 9e and f, which are denoted as HYB-I and HYB-II, respectively.

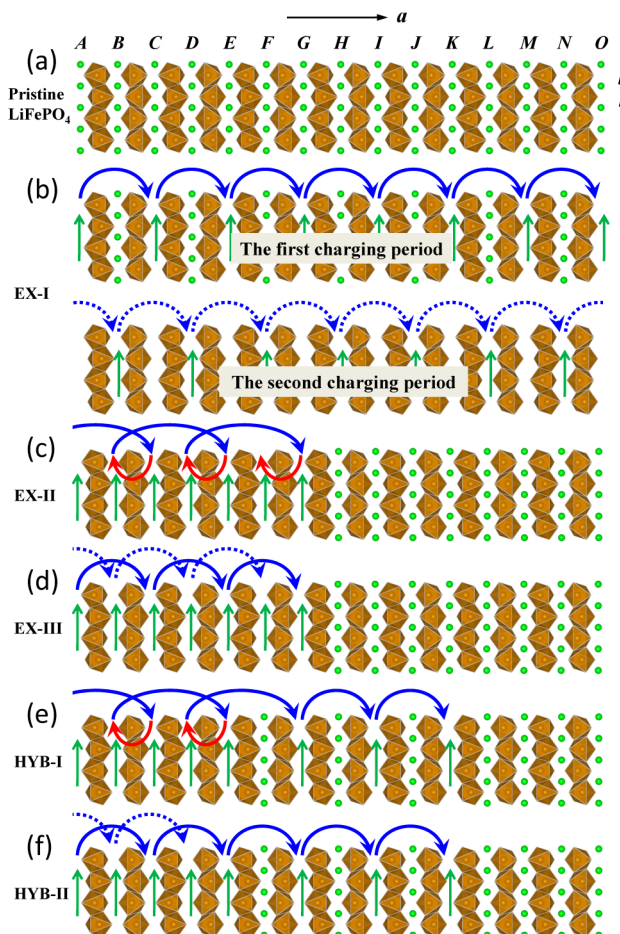


**Figure 9.** Schematic view of possible models for the electrochemical delithiation process of a single LiFePO<sub>4</sub> particle. Only FeO<sub>6</sub> octahedra (brown surfaces) and Li atoms (green balls) are shown for a convenient visualization. (a) Pristine LiFePO<sub>4</sub>, where Li layers are labeled in alphabetical order. (b) The EX-I model adopts the A–C–E–G–I delithiation sequence. (c) The EX-II model adopts the A–C–B–E–D delithiation sequence. (d) The EX-III model in which two delithiation waves move forward synchronously. (e) The HYB-I model hybridizing EX-I and EX-II. (f) A hybridized delithiation scheme of EX-I and EX-III, denoted by HYB-II. The green straight arrows refer to the Li diffusion path. The curved arrows represent the movement of the delithiation wave: the solid blue arrow and the solid red arrow refer to the first delithiation wave moving in the forward and backward directions, respectively; the dotted blue arrow refers to the second delithiation wave.

The HYB-I model is a simple hybridization of the EX-I model and the EX-II model. While the HYB-II model is a compromise between the two extreme models EX-I and EX-III: two delithiation waves coexist in a LiFePO<sub>4</sub> particle, but with the second one lagging behind the first one to some extent. Both of the HYB-I and HYB-II models result in a LiFePO<sub>4</sub>/stage-II/FePO<sub>4</sub> three-phase zone. A detailed analysis of all these models will be carried out in later sections. It should be stressed that here the phase boundaries are plotted to be perpendicular to the *a*-axis. In reality, this is not necessary, and the practical shape of phase boundary may be determined by other factors, such as the lattice defect or surface geometry.

We could anticipate the voltage profile on the basis of above delithiation models. The open circuit voltage is important not only because it is crucial for a battery system but also because it reflects the thermodynamic properties of the electrode material.

Figure 10 shows the corresponding voltage profile upon charging a small particle of LiFePO<sub>4</sub>. Even though a narrow

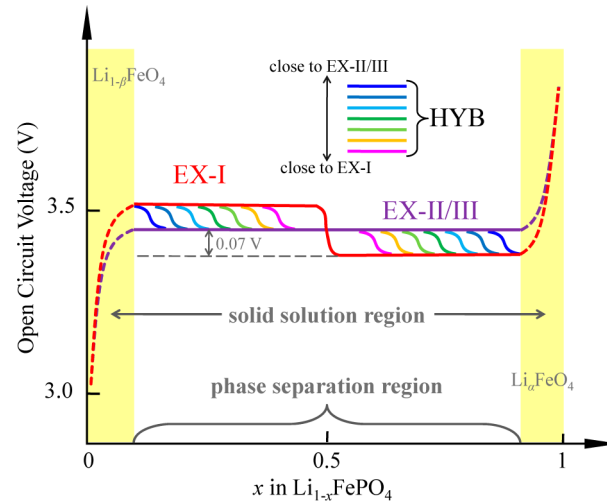


**Figure 10.** Hypothetical open circuit voltage profiles upon charging a single LiFePO<sub>4</sub> particle according to the delithiation models shown in Figure 9. For the phases in the solid state region, we use the notation proposed in ref 17. It should be stressed that here we take no account of the coherent strain effect induced by the lattice mismatch between different phases.

solid solution region is expected at the beginning and end of charging, we mainly focus on the phase separation region, where the phase boundary movement dominates the delithiation process. We have mentioned above that, according to the EX-I model, two charging periods should be expected. Thus, its voltage profile consists of two plateaus: the first one corresponds to the phase transition from LiFePO<sub>4</sub> to  $\text{Li}_{0.5}\text{FePO}_4$ , and the second one from  $\text{Li}_{0.5}\text{FePO}_4$  to FePO<sub>4</sub>. We may see that the first voltage plateau is 0.07 V higher than the average voltage of LiFePO<sub>4</sub> (3.45 V), while the second one is 0.07 V lower, contradicting the experimental results in which only one voltage plateau could be observed. Worse still, the voltage of the first plateau is higher than that of the second one, and this is by no means reasonable. The irrational voltage profile is not surprising, since the EX-I model is constructed only from the perspective of the lithium diffusion kinetics, while the thermodynamic limits are neglected. Figure 2 has shown that the formation energy of  $\text{Li}_{0.5}\text{FePO}_4$  with stage-II structure is 0.07 eV per formula unit higher than the separated LiFePO<sub>4</sub> and FePO<sub>4</sub> two phases, indicating the EX-I model is thermodynamically forbidden.

Although adopting different trajectories of delithiation, the EX-II and EX-III models are thermodynamically equivalent, as both of them lead to the same structure after delithiation, resulting in the same voltage profile. Figure 10 shows that the voltage keeps constant in the phase separation region, agreeing well with the experimental results. Furthermore, both of the EX-II and EX-III models could satisfy the thermodynamic and kinetic requirements simultaneously. However, the two models are overidealistic. For the EX-II model, the exactly back-and-forth delithiation sequence could be hardly achieved; the EX-III model requires that two delithiation waves strictly synchronize with each other, which is also less probable. Both of the two models bring about sharp LiFePO<sub>4</sub>/FePO<sub>4</sub> phase boundaries. However, no such experimental evidence has been found up to

now. We can prove in a later section that the sharp LiFePO<sub>4</sub>/FePO<sub>4</sub> two-phase boundary is not favored by the coherent strain resulted from the lattice mismatch. Therefore, neither the EX-II model nor the EX-III model is appropriate for describing the electrochemically delithiation process of a single LiFePO<sub>4</sub> particle.

Likewise, the voltage profile corresponding to the HYB-I and HYB-II models could also be plotted. As the HYB-I model and the HYB-II model are thermodynamically equivalent, we will use HYB to represent both models unless otherwise stated. The HYB model is a mix between the EX-I model and the EX-II/III model, and accordingly, its voltage profile depends on the ratio of EX-I and EX-II/III. Owing to the fact that the experimental voltage profile of LiFePO<sub>4</sub> has one remarkable plateau, the real model should be closer to EX-II/III than to EX-I. That is, the delithiation process is close to the thermodynamic equilibrium, which consists of separated LiFePO<sub>4</sub> and FePO<sub>4</sub> two phases, while there is a kinetically controlled structure, viz. the stage-II phase, between LiFePO<sub>4</sub> and FePO<sub>4</sub>. The resultant configuration is that a small quantity of stage-II phase situates between LiFePO<sub>4</sub> and FePO<sub>4</sub> two major phases, forming a three-phase zone. The three-phase zone has been directly observed through advanced STEM technique,<sup>26</sup> indicating that the HYB model is suitable for describing the microscopic delithiation process.

Theoretically, both the HYB-I model and the HYB-II model seem to be acceptable for describing the delithiation process of a single LiFePO<sub>4</sub> particle. However, the HYB-I model exhibits an elaborately designed delithiation sequence, which is analogous to the case of the EX-II model, and thus is less probable. By contrast, the HYB-II model depicts a more intuitive picture. According to the HYB-II model, there are two delithiation waves in a LiFePO<sub>4</sub> particle, analogous to the EX-I model and the EX-III model. The difference between the above three models lies in the degree of hysteresis between the first and the second delithiation waves. For the EX-I model, the second delithiation wave is initiated after the first one has gone through the whole particle, suggesting the largest hysteresis. For the EX-III model, there is no hysteresis between the two delithiation waves, as they are created simultaneously and then move together. The HYB-II model refers to a series of intermediate cases between the two extremes. As analyzed, it is more close to the EX-III model regarding a real delithiation process. Therefore, the hysteresis between the two delithiation waves should be small, but nonzero. Consequently, the size of the stage-II structure between LiFePO<sub>4</sub> and FePO<sub>4</sub>, as shown in Figure 9f, is limited. The HYB-II model could be characterized by two interfaces, that is, the LiFePO<sub>4</sub>/stage-II interface induced by the first delithiation wave and the FePO<sub>4</sub>/stage-II interface induced by the second delithiation wave. Accordingly, we may also call it the “dual-interface” model.

To simplify the calculation, we did not take account of the lattice strain effect accompanying the delithiation process, owing to the fact that the energy barrier of Li diffusion in LiFePO<sub>4</sub> shows less dependence on the lattice volume.<sup>51</sup> However, in a practical phase separation reaction, the lattice mismatch between the involved phases would unavoidably lead to interfacial stress on the phase boundary, and therefore, it has an impact on the dynamics of phase transition.<sup>53–56</sup> Experimental results have shown that the lattice volume extraction from LiFePO<sub>4</sub> to FePO<sub>4</sub> is 6.7%,<sup>3</sup> while DFT calculations underestimated this value to be ca. 5.0%.<sup>57</sup> As can be seen in Figure 11, the calculated lattice volume extraction

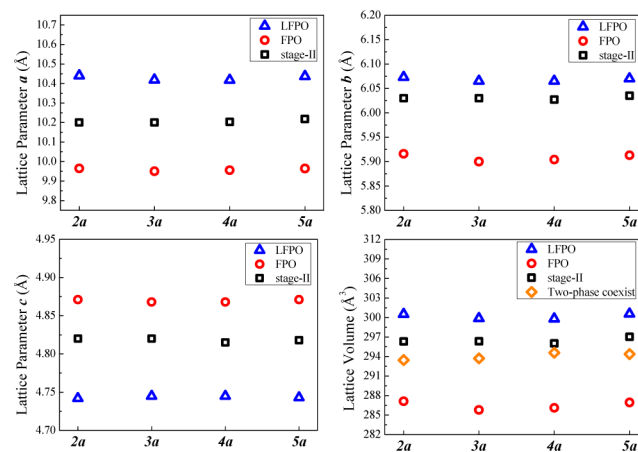


**Figure 11.** Calculated lattice parameters and volumes of LiFePO<sub>4</sub>, FePO<sub>4</sub>, and stage-II configurations. The lattice volume has been aligned to one formula unit of Li<sub>x</sub>FePO<sub>4</sub>. The naming rules follow the same scheme with that of Figure 2.

(vs LiFePO<sub>4</sub>) of stage-II (less than 1.5%) is not only much less than that of the fully delithiated phase FePO<sub>4</sub> (5.0%) but also smaller than the two-phase coexisting Li<sub>0.5</sub>FePO<sub>4</sub> supercell (more than 2.0%). Generally speaking, a smaller lattice volume change means less elastic misfit, and hence, it will facilitate the phase transformation.<sup>53</sup> In light of this trend, the stage-II structure may benefit from its intermediate lattice volume between LiFePO<sub>4</sub> and FePO<sub>4</sub> and thus act as a buffering phase to minimize the coherent strain. That is in accord with the scenario depicted in the dual-interface model, where the stage-II configuration situates between LiFePO<sub>4</sub> and FePO<sub>4</sub>. In contrast, the sharp LiFePO<sub>4</sub>/FePO<sub>4</sub> boundaries in the EX-II and EX-III models will increase the coherent strain to some extent; the HYB-I model also shares this disadvantage, as the sharp two-phase boundary will inevitably appear as an intermediate state. Once again, we show that the HYB-II model is the most appropriate one among all possible models shown in Figure 9.

Very recently, Liu et al. discovered the subtle but critical deviation from two-phase transformation exists in partially electrochemically delithiated LiFePO<sub>4</sub> through soft X-ray absorption spectroscopy, which is highly sensitive to the Fe 3d orbital such that a very low ratio of different Fe ions could be captured.<sup>58</sup> Their results suggest the appearance of an intermediate phase between LiFePO<sub>4</sub> and FePO<sub>4</sub>. This discovery, combined with the previous STEM observations,<sup>26</sup> further supports that the stage-II configuration is possibly situated between LiFePO<sub>4</sub> and FePO<sub>4</sub> two phases, which is in accordance with above delithiation model. The proportion of the intermediate phase could be very low, which rationalizes why this ordered Li staging structure could be revealed neither by diffraction imaging (X-ray or neutron), which reflected the information of an ensemble average and thereby is insensitive to minimum interface structure, nor by local atomic probe (e.g., hard X-ray absorption spectroscopy, Mössbauer Spectrometry, etc.) lacking sufficiently high resolution, in earlier research.

Note that all above discussion are based on phase separation scenario, where the step-by-step delithiation is expected as phase boundary propagation dominates the charging process. However, it has been reported that the two-phase nature of the LiFePO<sub>4</sub>/FePO<sub>4</sub> system changes into a one-phase solid-solution Li<sub>x</sub>FePO<sub>4</sub> system owing to the large anti-site disorder

induced by the specific processing method.<sup>22</sup> Dathar et al. proposed a concerted Li ion diffusion mechanism,<sup>51</sup> in which the interlayer Li transport is mediated by the Li–Fe anti-site defect. It may partly explain the solid-solution behavior mentioned. Nonetheless, we do not expect this mechanism to play a predominant role in a normal LiFePO<sub>4</sub> electrode, as the amount of antisite defects could be low after appropriate thermal treatment.<sup>59</sup> Recently, Oyama et al. showed that even for the defect-free LiFePO<sub>4</sub> electrode, the charge/discharge process could also exhibit nonequilibrium solid-solution character given the particles are small or the overpotential is large.<sup>60</sup> In the cases beyond two-phase reaction, the Li extraction may be initiated from multiple Li channels simultaneously rather than keep certain delithiation sequence and therefore may not be described using our delithiation model. Yet, the effective interlayer Li–Li interaction still plays an important role in delithiation process, even though the consequent Li diffusion behavior need to be further clarified.

The practical electrode material is a multiparticle ensemble, for which the complex particle–particle interactions could be considered. After relaxation, significant Li redistribution between various LiFePO<sub>4</sub> particles was observed.<sup>61</sup> Therefore, the charged electrode may consist of a collective of Li-rich and Li-poor particles, owing to a fast Li exchange between various particles to reach an energy minimum.<sup>62</sup> This effect is expected in the case that the charging rate is assumed to be much smaller than the Li relaxation rate between particles. The delithiation process for every single particle, before reaching the thermodynamic equilibrium of the whole multiparticle system, should follow the delithiation models proposed above.

## ■ DISCUSSION

By now, we may demonstrate that the Li staging in LiFePO<sub>4</sub> electrode is a thermodynamically metastable however kinetically controlled state, differing from the staging in GICs, which is considered to be thermodynamically favorable configuration mainly resulted from the direct Li<sup>+</sup>–Li<sup>+</sup> repulsive interactions.<sup>63</sup> Its formation could be ascribed to the Fe center mediated interlayer Li–Li interactions, which is closely related to the strong correlation nature of Fe 3d orbitals in LiFePO<sub>4</sub>. For other lithium intercalation materials with strongly correlated electron, such as the stage-II case in Li<sub>x</sub>FePO<sub>4</sub>, Li distribution at the interface could also be complex rather than an intuitive sharp phase boundary. For the system with weak correlation, it could be different. Taking Li<sub>4</sub>Ti<sub>5</sub>O<sub>12</sub> as an example, Ti ions exhibit weakly localized 3d electrons<sup>64</sup> and thus may invalidate the redox center mediated Li–Li interactions. Actually, a sharp Li<sub>4</sub>Ti<sub>5</sub>O<sub>12</sub>/Li<sub>7</sub>Ti<sub>5</sub>O<sub>12</sub> interface in a partially lithiated Li<sub>4</sub>Ti<sub>5</sub>O<sub>12</sub> has been observed by STEM techniques.<sup>65</sup> This is much different from the three-phase boundary in Li<sub>x</sub>FePO<sub>4</sub>.<sup>26</sup>

According to previous literature, Li–Li interactions have been taken into account in evaluating the Li diffusion kinetics of electrode materials exhibiting solid-solution behavior in the delithiation process (e.g., layered LiCoO<sub>2</sub>, LiTi<sub>2</sub>S<sub>2</sub>, or spinel LiMn<sub>2</sub>O<sub>4</sub>).<sup>66–68</sup> In these materials, the Li concentration can vary from dilute to fully concentrated limits, resulting in a strong concentration dependence of the Li diffusion coefficient.<sup>69</sup> While for the phase separation materials, such as spinel Li<sub>4</sub>Ti<sub>5</sub>O<sub>12</sub> or olivine LiFePO<sub>4</sub> discussed here, the Li concentration in solid solution phase is limited to a narrow region close to their stoichiometric end members (e.g., Li<sub>4</sub>Ti<sub>5</sub>O<sub>12</sub> and Li<sub>7</sub>Ti<sub>5</sub>O<sub>12</sub> for Li<sub>4+x</sub>Ti<sub>5</sub>O<sub>12</sub>) at room temperature.<sup>17,70</sup> For this reason, earlier theoretical researches on the

behavior of Li diffusion in these materials were usually carried out in a dilute vacancy limit, where the Li–Li interactions are ignored.<sup>8,9,71</sup> Such an approach may not have a problem with handling single phase (Li-rich or Li-poor phase for a typical two-phase reaction) reactions. Nevertheless, it needs to be emphasized that the major (de)lithiation process occur at the two-phase boundary in the phase separation system and thus could not be described by such a simplified treatment. Here, we show that, in LiFePO<sub>4</sub>, the Li diffusion kinetics is strongly dependent on the occupation of its adjacent Li layers, the cause of which lies in the fact that the effective oxidation state of charge centers will be determined by the arrangement of Li ion distribution and in turn have an impact on the behavior of Li ion diffusion. This implication highlights the importance of studying the phase boundary in understanding the delithiation mechanism.

After considering the interlayer Li–Li interactions, we may obtain a more comprehensive understanding of the delithiation process in a single LiFePO<sub>4</sub> particle. In a broader sense, the double-interface model proposed in this paper is not inconsistent with the widely accepted view that the reaction front is parallel to the *bc* plane and progresses in the *a* direction.<sup>14–16</sup> Nevertheless, it provides a more accurate description on the delithiation behavior near the generally believed two-phase boundary. In brief, the kinetic constraints force the delithiation to adopt an alternate layer way and thus leads to the stage-II phase, while the thermodynamic constraints tend to maintain LiFePO<sub>4</sub> and FePO<sub>4</sub> two phases and limit the growth of the energetically unfavorable stage-II phase. As a result, two delithiation waves, with one slightly lagging behind another, are needed to satisfy both the kinetic and thermodynamic requirements. Propagation of the two delithiation waves will lead to coexistence of three phases and two interfaces, explaining the cause of experimentally observed LiFePO<sub>4</sub>/stage-II/FePO<sub>4</sub> three-phase zone.

## ■ CONCLUSION

In summary, we have performed first-principles calculations in the GGA+U framework to show that the observed lithium staging configuration in partially delithiated LiFePO<sub>4</sub> is a kinetically controlled thermodynamically metastable state, which is distinct from the well-known staging phenomenon in GICs. After one Li layer is empty, the resulting asymmetry of two prior equivalent Fe centers in the adjacent Li layer will lead to a high small polaron barrier and thus inhibit the Li diffusion. Consequently, a facile lithium extraction will be much more likely to happen in the second nearest Li layer. That is, the lithium extraction prefers an alternate layer way rather than the sequential layer-by-layer way, rationalizing the experimentally observed stage-II configuration. Accordingly, we proposed a double-interface model to describe the microscopic delithiation process. Based on this model, two asynchronous delithiation waves are formed and then propagate across the LiFePO<sub>4</sub> particle. Thus, a LiFePO<sub>4</sub>/stage-II/FePO<sub>4</sub> three-phase zone with two interfaces is formed upon charging. Our model successfully explains recent experimental observations at the atomic scale. All these phenomena originate from the strong electron correlation of Fe ions in LiFePO<sub>4</sub>, through which the indirect interlayer Li–Li interaction is constructed. For other Li intercalation materials with strongly correlated electrons, analogous interactions could also be expected. Therefore, the insights from this study not only provide fundamental understanding of Li diffusion kinetics in LiFePO<sub>4</sub> cathode

material but also shed light on the interactions between electron and ion and hence may have general implications for investigating the ionic transport in other strongly correlated mixed conductor materials. Our results reveal that the Li diffusion kinetics is essential to determine the phase boundary structure at least for the phase separation materials.

## AUTHOR INFORMATION

### Corresponding Author

\*E-mail: xjhuang@iphy.ac.cn.

### Notes

The authors declare no competing financial interest.

## ACKNOWLEDGMENTS

The authors thank Prof. Lin Gu for fruitful discussions. The calculations are partially finished at the Virtual Laboratory for Computational Chemistry, Computer Network Information Center, Chinese Academy of Sciences. This work has been supported by “973” projects (2009CB220100, 2012CB932900) and CAS (KJCX2-YW-W26).

## REFERENCES

- (1) Armand, M.; Tarascon, J. M. *Nature* **2008**, *451*, 652.
- (2) Ellis, B. L.; Lee, K. T.; Nazar, L. F. *Chem. Mater.* **2010**, *22*, 691.
- (3) Padhi, A. K.; Nanjundaswamy, K. S.; Goodenough, J. B. *J. B. J. Electrochem. Soc.* **1997**, *144*, 1188.
- (4) Andersson, A. S.; Kalska, B.; Haggstrom, L.; Thomas, J. O. *Solid State Ion.* **2000**, *130*, 41.
- (5) Ravet, N.; Chouinard, Y.; Magnan, J. F.; Besner, S.; Gauthier, M.; Armand, M. *J. Power Sources* **2001**, *97–8*, 503.
- (6) Herle, P. S.; Ellis, B.; Coombs, N.; Nazar, L. F. *Nat. Mater.* **2004**, *3*, 147.
- (7) Kang, B.; Ceder, G. *Nature* **2009**, *458*, 190.
- (8) Morgan, D.; Van der Ven, A.; Ceder, G. *Electrochem. Solid State Lett.* **2004**, *7*, A30.
- (9) Ouyang, C. Y.; Shi, S. Q.; Wang, Z. X.; Huang, X. J.; Chen, L. Q. *Phys. Rev. B* **2004**, *69*, 104303.
- (10) Islam, M. S.; Driscoll, D. J.; Fisher, C. A. J.; Slater, P. R. *Chem. Mater.* **2005**, *17*, 5085.
- (11) Nishimura, S.; Kobayashi, G.; Ohoyama, K.; Kanno, R.; Yashima, M.; Yamada, A. *Nat. Mater.* **2008**, *7*, 707.
- (12) Andersson, A. S.; Thomas, J. O. *J. Power Sources* **2001**, *97–8*, 498.
- (13) Srinivasan, V.; Newman, J. *J. Electrochem. Soc.* **2004**, *151*, A1517.
- (14) Delmas, C.; Maccario, M.; Croguennec, L.; Le Cras, F.; Weill, F. *Nat. Mater.* **2008**, *7*, 665.
- (15) Chen, G. Y.; Song, X. Y.; Richardson, T. J. *Electrochem. Solid State Lett.* **2006**, *9*, A295.
- (16) Laffont, L.; Delacourt, C.; Gibot, P.; Wu, M. Y.; Kooyman, P.; Masquelier, C.; Tarascon, J. M. *Chem. Mater.* **2006**, *18*, 5520.
- (17) Yamada, A.; Koizumi, H.; Nishimura, S. I.; Sonoyama, N.; Kanno, R.; Yonemura, M.; Nakamura, T.; Kobayashi, Y. *Nat. Mater.* **2006**, *5*, 357.
- (18) Meethong, N.; Huang, H. Y. S.; Carter, W. C.; Chiang, Y. M. *Electrochem. Solid State Lett.* **2007**, *10*, A134.
- (19) Kobayashi, G.; Nishimura, S. I.; Park, M. S.; Kanno, R.; Yashima, M.; Ida, T.; Yamada, A. *Adv. Funct. Mater.* **2009**, *19*, 395.
- (20) Ellis, B.; Perry, L. K.; Ryan, D. H.; Nazar, L. F. *J. Am. Chem. Soc.* **2006**, *128*, 11416.
- (21) Dodd, J. L.; Yazami, R.; Fultz, B. *Electrochem. Solid State Lett.* **2006**, *9*, A151.
- (22) Gibot, P.; Casas-Cabanas, M.; Laffont, L.; Levasseur, S.; Carlach, P.; Hamelet, S.; Tarascon, J. M.; Masquelier, C. *Nat. Mater.* **2008**, *7*, 741.
- (23) Gu, L.; Zhu, C. B.; Li, H.; Yu, Y.; Li, C. L.; Tsukimoto, S.; Maier, J.; Ikuhara, Y. *J. Am. Chem. Soc.* **2011**, *133*, 4661.
- (24) Zhou, F.; Maxisch, T.; Ceder, G. *Phys. Rev. Lett.* **2006**, *97*, 155704.
- (25) Malik, R.; Zhou, F.; Ceder, G. *Nat. Mater.* **2011**, *10*, 587.
- (26) Suo, L.; Han, W.; Lu, X.; Gu, L.; Hu, Y. S.; Li, H.; Chen, D.; Chen, L.; Tsukimoto, S.; Ikuhara, Y. *Phys. Chem. Chem. Phys.* **2012**, *14*, 5363.
- (27) Singh, G. K.; Ceder, G.; Bazant, M. Z. *Electrochim. Acta* **2008**, *53*, 7599.
- (28) Burch, D.; Bazant, M. Z. *Nano Lett.* **2009**, *9*, 3795.
- (29) Wagemaker, M.; Singh, D. P.; Borghols, W. J. H.; Lafont, U.; Haverkate, L.; Peterson, V. K.; Mulder, F. M. *J. Am. Chem. Soc.* **2011**, *133*, 10222.
- (30) Bai, P.; Cogswell, D. A.; Bazant, M. Z. *Nano Lett.* **2011**, *11*, 4890.
- (31) Zhu, Y.; Wang, C. *J. Phys. Chem. C* **2010**, *114*, 2830.
- (32) Kresse, G.; Furthmüller, J. *Phys. Rev. B* **1996**, *54*, 11169.
- (33) Kresse, G.; Furthmüller, J. *Comput. Mater. Sci.* **1996**, *6*, 15.
- (34) Blochl, P. E. *Phys. Rev. B* **1994**, *50*, 17953.
- (35) Perdew, J. P.; Burke, K.; Ernzerhof, M. *Phys. Rev. Lett.* **1996**, *77*, 3865.
- (36) Bengone, O.; Alouani, M.; Blochl, P.; Hugel, J. *Phys. Rev. B* **2000**, *62*, 16392.
- (37) Liechtenstein, A. I.; Anisimov, V. I.; Zaanen, J. *Phys. Rev. B* **1995**, *52*, R5467.
- (38) Zhou, F.; Cococcioni, M.; Marianetti, C. A.; Morgan, D.; Ceder, G. *Phys. Rev. B* **2004**, *70*, 235121.
- (39) Zhou, F.; Kang, K. S.; Maxisch, T.; Ceder, G.; Morgan, D. *Solid State Commun.* **2004**, *132*, 181.
- (40) Fisher, C. A. J.; Prieto, V. M. H.; Islam, M. S. *Chem. Mater.* **2008**, *20*, 5907.
- (41) Meng, Y. S.; Arroyo-de Domínguez, M. E. *Energy Environ. Sci.* **2009**, *2*, 589.
- (42) Gardiner, G. R.; Islam, M. S. *Chem. Mater.* **2010**, *22*, 1242.
- (43) Lee, J. W.; Zhou, W.; Idrobo, J. C.; Pennycook, S. J.; Pantelides, S. T. *Phys. Rev. Lett.* **2011**, *107*, 085507.
- (44) Henkelman, G.; Überuaga, B. P.; Jonsson, H. *J. Chem. Phys.* **2000**, *113*, 9901.
- (45) Maxisch, T.; Zhou, F.; Ceder, G. *Phys. Rev. B* **2006**, *73*, 104301.
- (46) Fischer, J. E.; Thompson, T. E. *Phys. Today* **1978**, *31*, 36.
- (47) Dresselhaus, M. S.; Dresselhaus, G. *Adv. Phys.* **1981**, *30*, 139.
- (48) Ohzuku, T.; Iwakoshi, Y.; Sawai, K. *J. Electrochem. Soc.* **1993**, *140*, 2490.
- (49) Zaghib, K.; Mauger, A.; Goodenough, J. B.; Gendron, F.; Julien, C. M. *Chem. Mater.* **2007**, *19*, 3740.
- (50) Asari, Y.; Suwa, Y.; Hamada, T. *Phys. Rev. B* **2011**, *84*, 134113.
- (51) Dathar, G. K. P.; Sheppard, D.; Stevenson, K. J.; Henkelman, G. *Chem. Mater.* **2011**, *23*, 4032.
- (52) Zhou, F.; Marianetti, C. A.; Cococcioni, M.; Morgan, D.; Ceder, G. *Phys. Rev. B* **2004**, *69*.
- (53) Meethong, N.; Huang, H. Y. S.; Speakman, S. A.; Carter, W. C.; Chiang, Y. M. *Adv. Funct. Mater.* **2007**, *17*, 1115.
- (54) Van der Ven, A.; Garikipati, K.; Kim, S.; Wagemaker, M. J. *Electrochem. Soc.* **2009**, *156*, A949.
- (55) Zhu, Y.; Wang, C. *J. Power Sources* **2011**, *196*, 1442.
- (56) Cogswell, D. A.; Bazant, M. Z. *ACS Nano* **2012**, *6*, 2215.
- (57) Zhou, F.; Cococcioni, M.; Kang, K.; Ceder, G. *Electrochem. Commun.* **2004**, *6*, 1144.
- (58) Liu, X.; Liu, J.; Qiao, R.; Yu, Y.; Li, H.; Suo, L.; Hu, Y.-S.; Chuang, Y.-D.; Shu, G.; Chou, F.; Weng, T.-C.; Nordlund, D.; Sokaras, D.; Wang, Y. J.; Lin, H.; Barbiellini, B.; Bansil, A.; Song, X.; Liu, Z.; Yan, S.; Liu, G.; Qiao, S.; Richardson, T. J.; Prendergast, D.; Hussain, Z.; de Groot, F. M. F.; Yang, W. *J. Am. Chem. Soc.* **2012**, *134*, 13708.
- (59) Chen, J. J.; Bai, J. M.; Chen, H. Y.; Graetz, J. *J. Phys. Chem. Lett.* **2011**, *2*, 1874.
- (60) Oyama, G.; Yamada, Y.; Natsui, R.-i.; Nishimura, S.-i.; Yamada, A. *J. Phys. Chem. C* **2012**, *116*, 7306.
- (61) Lee, K. T.; Kan, W. H.; Nazar, L. F. *J. Am. Chem. Soc.* **2009**, *131*, 6044.

- (62) Dreyer, W.; Jamnik, J.; Guhlke, C.; Huth, R.; Moskon, J.; Gaberscek, M. *Nat. Mater.* **2010**, *9*, 448.
- (63) Persson, K.; Hinuma, Y.; Meng, Y. S.; Van der Ven, A.; Ceder, G. *Phys. Rev. B* **2010**, *82*, 125416.
- (64) Chevrier, V. L.; Ong, S. P.; Armiento, R.; Chan, M. K. Y.; Ceder, G. *Phys. Rev. B* **2010**, *82*, 075122.
- (65) Lu, X.; Zhao, L.; He, X.; Xiao, R.; Gu, L.; Hu, Y.-S.; Li, H.; Wang, Z.; Duan, X.; Chen, L.; Maier, J.; Ikuhara, Y. *Adv. Mater.* **2012**, *24*, 3233.
- (66) Van der Ven, A.; Ceder, G.; Asta, M.; Tepesch, P. D. *Phys. Rev. B* **2001**, *64*, 184307.
- (67) Van der Ven, A.; Thomas, J. C.; Xu, Q.; Swoboda, B.; Morgan, D. *Phys. Rev. B* **2008**, *78*, 104306.
- (68) Xu, B.; Meng, S. *J. Power Sources* **2010**, *195*, 4971.
- (69) Van der Ven, A.; Bhattacharya, J.; Belák, A. A. *Acc. Chem. Res.* **2012**, DOI: 10.1021/ar200329r.
- (70) Wagemaker, M.; Simon, D. R.; Kelder, E. M.; Schoonman, J.; Ringpfeil, C.; Haake, U.; Lutzenkirchen-Hecht, D.; Frahm, R.; Mulder, F. M. *Adv. Mater.* **2006**, *18*, 3169.
- (71) Chen, Y. C.; Ouyang, C. Y.; Song, L. J.; Sun, Z. L. *Electrochim. Acta* **2011**, *56*, 6084.